AIAA JOURNAL
Vol. 43, No. 5, May 2005

Fast Fourier Transform Convergence Criterion for Numerical Simulations of Periodic Fluid Flows

Mohamed H. Ahmed* and Thomas J. Barber†
University of Connecticut, Storrs, Connecticut 06269

Determining when a numerical simulation is fully converged is important in getting accurate and reliable results. In unsteady problems, especially those involving periodic flows, it is not easy to judge convergence based on the existing convergence criteria. In this study, a convergence criterion based on an analysis of the frequency content of several flow variables using the fast Fourier transform (FFT) is suggested. This FFT convergence criterion has an advantage in that it is based on evaluation of the physical flow variables. Two conditions are set to judge convergence using the FFT convergence criterion. The first condition deals with the errors associated with the selection of the number of samples, whereas the other deals with the physical frequencies and their amplitudes. The FFT convergence criterion is tested and applied to two different unsteady flow problems, which have been solved numerically using two different flow solver codes. The results show that the suggested FFT convergence criterion can be applied successfully and easily to judge the degree of convergence of numerical simulations of periodic fluid flows.

Nomenclature

A	=	normalized amplitude
Dt	=	sampling rate
d	=	hydraulic diameter of jet, m
f	=	frequency, Hz
H	=	computational domain height, m
J	=	momentum flux ratio
L	=	computational domain length, m
N	=	number of data
p	=	point
Sr	=	Strouhal number
t	=	time, s
u	=	axial-velocity component, m/s
v	=	vertical-velocity component, m/s
W	=	computational domain depth, m
w	=	spanwise-velocity component, m/s
x	=	axial distance, m
y	=	vertical distance, m
z	=	spanwise distance, m

Subscripts

c	=	cutoff
ds	=	data samples
eb	=	error band
FFT	=	fast Fourier transform
max	=	maximum
p	=	predicted
sp	=	spacing
1	=	error frequency
2	=	dominant physical frequency
3	=	secondary physical frequency

Received 3 December 2003; presented as Paper 2004-0738 at the AIAA 42nd Aerospace Sciences Meeting, Reno, NV, 5–8 January 2004; revision received 13 December 2004; accepted for publication 14 December 2004.

*Graduate Student, Department of Mechanical Engineering; currently Assistant Professor, Mechanical Engineering Department, Faculty of Engineering, Assiut University, Assiut 71516, Egypt.

†Professor in Residence, Department of Mechanical Engineering. Associate Fellow AIAA.

Introduction

NUMERICAL simulation has become an essential tool used in solving problems in many scientific areas. In many cases, it is less expensive and time consuming when compared to an experimental approach. An analyst should be able to demonstrate that their numerical solutions are fully converged. An examination of the frequency content has become an important tool to analyze and understand the physical characteristics of unsteady periodic flow problems.[1–5] Periodic unsteadiness in the flowfield can occur naturally, for example, the shedding of recirculation eddies behind bluff bodies to form a von Kármán vortex street and the growth of instabilities in a shear layer as in case of jet flows. Periodic unsteadiness can also occur when forcing is imposed on one or more of the flow boundaries. In such unsteady flow problems, judging if a solution has converged is necessary in determining the correct spectral content of the solution.

Convergence refers to two issues in numerical simulations. The first is the iteration convergence, defined by Roache and others[6–9] as finally arriving at a solution of a finite difference equation via iteration. Iteration can be defined as the solution of the discretized governing equations over the computational domain. The second issue is called truncation convergence, which is the convergence of the discretized equation to the partial differential equation as time step and grid size go to zero. In this work, the word convergence refers to iteration convergence. Convergence criteria are typically based on examining local parameters at each cell or node, for example, residuals of the governing equations or specific flow variables. The residual represents the inability to satisfy the governing equations at a particular iteration step. Typically, one considers the change of a residual or a flow variable from two consecutive time steps at a particular node or forms an rms sum of these quantities over the entire computational domain. Sometimes these parameters are normalized, but there is a risk if the parameter becomes locally small. Convergence criteria can also be categorized into two separate groups: ones that are evaluated on the boundaries of the computational domain, whereas others are evaluated at the local nodes or control volume. The first category examines the global parameters such as the mass balance across a given boundary or the temperature[10] on a given boundary. The advantage of a mass balance convergence criterion is that it measures an actual physical property. A similar physics-based criterion has been developed and applied for reacting flow computations, where one tracks the total number of atoms of a given element to obtain another measure of convergence.[11] Mathematically, convergence has been defined[7,8] as when the difference between an actual variable and its discretized

approximation goes to zero, as the mesh spacing goes to zero and the iteration indices go to infinity. In practice, the mesh does not get that small, and one does not want to iterate forever.

Roache[6] presented an assessment of some of various forms of convergence criteria, where convergence is said to be reached if 1) the value of a residual drops below a specified value, for example, $\varepsilon \approx \mathcal{O}(10^{-3} - 10^{-8})$; 2) a residual is "monotonically" decreasing; and 3) the flowfield looks unchanged from the solution at some earlier iteration. Such an approach to examine convergence is suitable for steady-state simulations, where residuals can decrease monotonically. A residual does not have to go to zero because calculations are performed using a finite mesh size and algorithmic details lead to additional errors. Changing the mesh changes the residual error and therefore makes the convergence cutoff level mesh dependent. Roache therefore states that there is little rationale for choosing when convergence is achieved and that the choice of criteria and its level are largely subjective.

For unsteady flows, the finite spatial and temporal (inner loop) mesh causes the convergence cutoff value to exhibit mesh dependency. In case of periodic flow problems, the residual change is larger than compared to the residual for a steady-state case, and furthermore the residual is most likely to be periodic. Even when the residual fluctuates periodically below the specified value, the pattern of fluctuations can change as the solution runs further. Therefore, for periodic flow problems there is a question about what should be the specified value to judge convergence. A new convergence criterion is offered to help judging convergence of these types of problems.

One subcategory of unsteady flows is called periodic. Periodic fluid flow behavior can occur naturally, as in the case of turbulent flow over bluff bodies and flow over cavities, or if one or more of the boundaries are forced to have a periodic behavior. For unsteady turbulent flows, flowfield variables can be broken down to a time-averaged part, a quasi-periodic, or coherent part and an incoherent or random part. The first term corresponds to the global mean flow. The second term, called the deterministic term, is defined by timescales related to the motion of large-scale or coherent structures. The third term, called the stochastic or turbulence term, is defined by the timescale of turbulent eddy motion. The sprit of this decomposition is similar to that first proposed by Reynolds and Hussain[12] and subsequently by others.[13,14] The first two terms can be resolved without modeling by many practical numerical methods. Abbott and Basco[9] reviewed some of the applications (which can include unsteadiness) where the k–ε model was used successfully. Applications include sudden expansions, flows around an obstacle, cavity flows, and jets in crossflow. The resolvable large scales move very slowly and have a long length and timescales in comparison to the irresolvable turbulent small scales (small length and timescales). This suggests using the two-equation closure models to solve unsteady problems when the main concern is to obtain a solution for the unsteady resolvable large scale (as is the case in the present study). The k–ε model has been used successfully to simulate problems such as flow over bluff bodies.[15,16]

The aim of this study is to examine an alternative convergence criterion based on a fast Fourier transform (FFT) frequency analysis of several flow variables. This convergence criterion is for periodic fluid flows. The FFT results are examined to study the effect of different FFT parameters on the calculated frequencies and their amplitudes. To apply and investigate the FFT convergence criterion, two different flow problems are solved numerically using two different codes. The first problem is an analysis of a forced jet injected into a crossflow, where the unsteady periodic flow behavior arises from forcing one of the boundaries with a sinusoidal waveform frequency. The second problem is an analysis of the flow over a triangular flame holder, where periodic unsteadiness occurs naturally as a result of shedding of the fluid flow from a boundary surface. Based on the work just cited, the present study also models the unsteady turbulent scales using two-equation models.

FFT Convergence Criterion

The suggested alternative convergence criterion is based on examining the frequencies and amplitudes (using FFT analysis) of selected variables at points distributed throughout the computational domain. Data samples are collected over a number of time steps, and the frequencies and their amplitudes are calculated and examined as the solution progresses in time. Using this type of analysis, two types of frequencies can be easily identified. The first type depends on the number of data samples and sampling rate used in the FFT method, defined herein as the error frequency. This error frequency is the largest amplitude signal in the cutoff region, and its amplitude can be interpreted as a measure of how the overall solution has converged (see next section for details). The second type includes all of the physical frequencies of the solution that exist outside of the cutoff region. From these physical frequencies, there is at least one frequency that has an amplitude which is dominant over the spectral range (dominant energy).

The unsteady convergence criterion using this approach is defined as satisfying the following two conditions:

1) The amplitude of the dominant frequency in the cutoff region "dominant error frequency" is very small compared to the amplitudes of the physical frequencies of the problem.

2) The change in the physical frequencies and their amplitudes is less than specified small value.

Because this convergence criterion examines the frequency content of the solution space, these frequencies should be well defined. This convergence criterion can be applied to both periodic laminar and turbulent flows. In the case of turbulent flow, the large-scale eddies have nonrandom frequency values, and they are used in the FFT convergence analysis. The small-scale eddies also have random frequency content and cannot be used for FFT convergence criterion. A detailed FFT algorithm and FORTRAN code can be found in Proakis.[17] In this study, the FFT analysis has been computed using MATLAB® software.[18]

Three numerical simulations are analyzed to demonstrate the proposed method. The first one is a test problem where a known signal in the time domain is analyzed using FFT to examine the effect of the number of data samples, the number of FFT points, and the sampling rate on the solution obtained from the FFT analysis. The other two cases are real periodic fluid flow problems: 1) the forced jet in crossflow and 2) the flow over a triangular flame holder.

Fast Fourier Transform

FFT is an efficient mathematical method to compute the discrete Fourier transform (DFT). DFT plays an important role in many applications of digital signal processing. If $x(n)$ is a sequence defined only over the interval from 0 to $N-1$, the DFT, $X(k)$, of $x(n)$ is defined[19] only over the same interval from 0 to $N-1$.

$$X(k) = \sum_{n=0}^{N-1} x(n)\, e^{-ik\omega_0 n}, \qquad 0 \le k \le N-1 \tag{1}$$

where $i = \sqrt{-1}$, $\omega_0 = 2\pi/N$ (radians), and k is called frequency index. The preceding relation can be rewritten as

$$X(k) = \sum_{n=0}^{N-1} x(n)\, W_N^{kn}, \qquad 0 \le k \le N-1 \tag{2}$$

where $W_N = e^{-2\pi i/N}$ is called the phase factor. The total multiplication processes are $4N2$ ($4N$ for each value of k) and $N(4N-2)$ addition processes [$4(N-1)+2$ for each value of k]. These processes are very computational expensive if N is large. The FFT method reduces the number of the multiplication processes (usually more critical than the addition processes[7]). The FFT technique assumes that the N points are a power of 2, that is, $N = 2^{\beta}$. The FFT method breaks the N-point transform into two $(N/2)$-point transform and then breaks the $(N/2)$-point transform into two $(N/4)$-point transform and so on. For example, for the first break, $(N/2)$-point transform, the number of multiplication processes is $N^2/2 + N$. For the second break, $N/4$-point transform, the number of multiplication preceding is $N^2/4 + 2N$. The preceding processes can be continued to β stages or $\log_2 N$ stages. The total number of multiplication

processes in this case is $(N/2)\log_2 N$, and the number of addition processes is $N \log_2 N$. To show how fast FFT compared with DFT, assume $N = 2^{10}$ $(N = 1024)$. The number of multiplication processes using DFT is 10,048,576, whereas for FFT it is 5,120. FFT is 205 faster than the DFT.

Zero padding is adding zeros to the end of a sequence of finite length so that a power of 2 FFT algorithm can be used. Another advantage of zero padding is that the samples values are spaced $2\pi/(N_f + N_z)$, where N_f is the number of the nonzero points of the original sequence and N_z is the number of zeros added to the original sequence. Adding more zeros provides closer spaced samples and gives a better display of the Fourier transform.[19] The amplitude of the frequency domain is a function not only of the amplitude of the original signal (A_0) but also of the number of FFT points (N_{FFT}) as $A = A_0\, N/2$. The frequency (f_k, Hz) can be calculated[7] as

$$f_k = k/N\,\Delta T \tag{3}$$

The FFT is a mathematical method to change the signal value from the time domain into the frequency domain. The maximum frequency that can be captured using FFT depends on the sampling rate used and can be calculated from

$$f_{\text{FFT, max}} = 1/2\,\Delta t \tag{4}$$

where Δt is the sampling rate. The spacing frequency value, which can be defined as the difference between two consecutive frequencies calculated using FFT, is found from

$$f_{\text{sp}} = 1/\,N_{\text{FFT}}\Delta t \tag{5}$$

where N_{FFT} is the number of data points used in the FFT analysis and should be a power of 2. Also, N_{FFT} should be equal or larger than the number of data samples. When the number of the data samples is the same as the number of FFT points, the frequencies calculated have an error band that can be calculated from

$$f_{\text{eb}} = \tfrac{1}{2}(1/N_{\text{FFT}}\,\Delta t) \tag{6}$$

When the number of FFT points does not equal the number of the data samples, Eq. (6) gives fair results.

The correct frequency is within the following frequency range:

$$f = f_p \pm f_{\text{eb}} \tag{7}$$

The cutoff frequency, which is defined here as the minimum frequency that can be captured correctly using FFT, depends on the number of data samples N_{ds} and the sampling rate Δt. It is calculated from

$$f_c = 1/N_{\text{ds}}\Delta t \tag{8}$$

Sometimes the error frequency is calculated to occur outside of the cutoff region, and it is not possible to identify it as an error frequency. During early stages of a simulation, the frequency content of the signal at a certain point has some frequencies that are different from the physical frequencies that can exceed twice the cutoff frequency. Therefore, in the present study of the FFT convergence criterion the cutoff region is doubled from that of Eq. (8) to avoid terminating the calculation before real convergence has been obtained. Again, if the number of FFT points does not equal the number of data samples, the effect of the error band on the calculated error frequency can sometimes be little higher than that calculated by Eq. (8). Therefore, this shifts the error frequency out of the cutoff region.

In this study, the cutoff region is defined as the region in the frequency domain where the maximum frequency is the cutoff frequency, calculated using Eq. (8).

Results

Three numerical simulations are examined to demonstrate the proposed procedure. The first provides a calibration of the procedure by analyzing a complex signal composed of analytically generated unsteady signals. The second simulation of a forced jet in crossflow examines the behavior of an imposed unsteady signal of the flow and convergence characteristics. Finally, a simulation of flow-induced unsteadiness is examined.

Analytical Example

Four different test cases are used to understand the errors caused by the FFT method parameters. In each case, a known signal of three different frequencies is imposed and analyzed. The known signal is of the form

$$y = \sum_1^3 y_i = \sum_1^3 A_i \sin(2\pi f_i t) \tag{9}$$

In these four cases, the values of the normalized amplitudes (A_1, A_2, A_3) are 0.5, 1.0, and 0.75, and the second and third frequency values (f_2 and f_3) are 400 and 600 Hz. The sampling rate is 0.1 ms. Table 1 shows the value of the first imposed frequency $f_{i,1}$ or one of FFT method parameters changes in each case. The table shows the value of the first input frequency $f_{i,1}$, the predicted values of the frequencies and normalized amplitudes, the number of FFT point N_{FFT}, the number of data samples N_{ds}, the maximum error in FFT Δf_{eb}, the maximum error between the predicted and the input frequencies $\Delta f_{c,\max}$, and at the end, the value of the cutoff frequency respectively f_c.

In the first FFT case study, the value of f_1 is 70 Hz, and the sampling rate is 0.1 ms, that is, 10,000 data samples. Figure 1 shows a part of the $y(t)$ signal in the time domain. Figure 2 shows the same signal in the frequency domain using 10,000 data samples and 2^{20} FFT data. The FFT analysis accurately predicts the frequencies, the normalized amplitudes of the imposed signal, and the cutoff frequency (1 Hz in this case). The number of FFT data must be a multiple of 2 and equal to or higher than the number of data samples. The number of data samples can be any value greater than 1; however, the larger the number of data samples, the more accurate the obtained frequencies. In applying the FFT convergence criterion, it is recommended that the number of data samples be a multiple of 2 whenever possible.

The effect of N_{ds}, as well as N_{FFT}, on the FFT convergence criterion needs to be investigated in greater detail. Using the waveform shape given by Eq. (4), case 2, with 256 points for the data samples and 256 for the FFT points, illustrates that the cutoff frequency is 39.06 Hz, and the accuracy of the predicted frequencies is

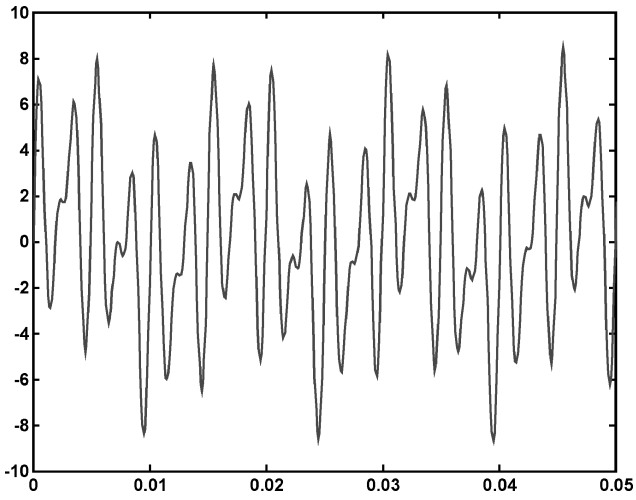

Fig. 1 Signal value in the time domain of the combined sine waves of 70, 400, and 600 Hz with normalized amplitudes of 0.50, 1.00, and 0.75, respectively.

Table 1 Values of different parameters test cases used to study FFT method

Test case no.	$f_{i,1}$	Predicted frequencies, Hz			Predicted normalized amplitudes			N_{FFT}	N_{ds}	$\pm\Delta f_{\text{eb}}$	$\pm\Delta f_{c,\max}$	f_c
		$f_{p,1}$	$f_{p,2}$	$f_{p,3}$	$A_{p,1}$	$A_{p,2}$	$A_{p,3}$					
1	70	69.99	400.0	600.0	0.500	1	0.750	2^{20}	10^4	0.005	0.00	1
2	70	78.10	390.6	585.9	0.474	1	0.591	256	256	19.53	14.1	39.06
3	70	67.60	398.1	602.0	0.507	1	0.757	2^{20}	256	0.005	2.4	39.06
4	15	39.06	390.6	585.9	0.154	1	0.594	256	256	19.53	14.1	39.06
5	15	36.20	398.5	602.5	0.144	1	0.769	2^{20}	256	0.005	2.50	39.06

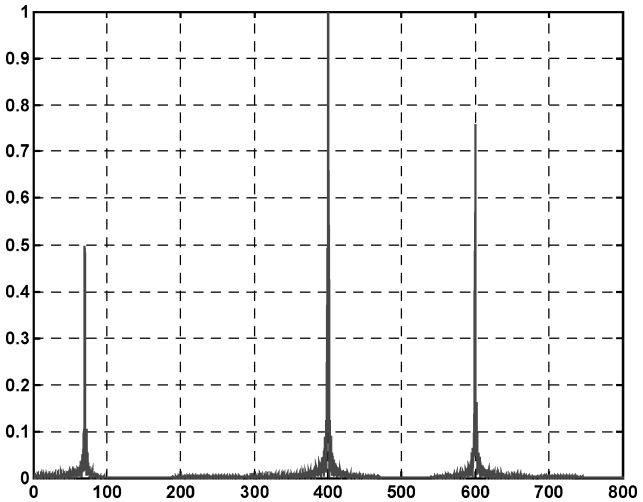

Fig. 2 FFT analysis of the signal value is shown in Fig. 1 using $N_{\text{ds}} = 10{,}000$ and $N_{\text{FFT}} = 2^{20}$.

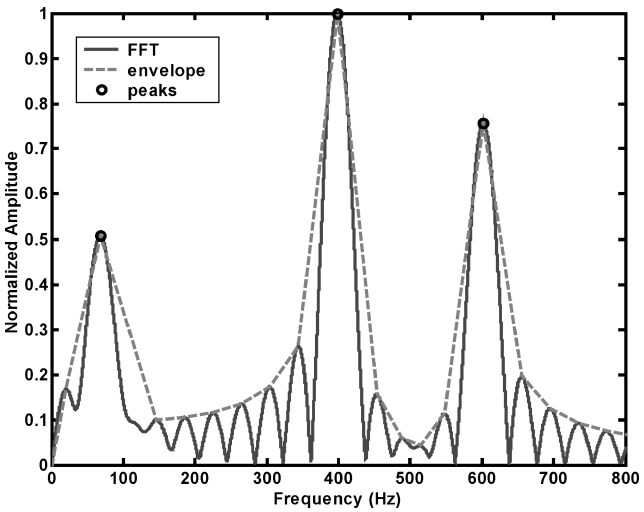

Fig. 3 FFT analysis, envelope, and peaks of signal value using $N_{\text{ds}} = 256$ and $N_{\text{FFT}} = 2^{20}$ (case 3).

within ± 19.53 Hz. The normalized amplitudes however are lower than the correct values. For case 3, the predicted frequencies and amplitudes are more accurate than in case 2. The maximum difference between the predicted and the input frequencies is 2.4 Hz, which is lower than the 9.4 Hz of case 2. The location of this maximum discrepancy changes from the 400 Hz of case 2 to the 70 Hz of case 3. In case 4, the value of the first frequency f_1 changes from 70 Hz to a value below the cutoff of 39.06 Hz (for example, 15 Hz), and its amplitude is lower than the input 0.5 value. In case 5, the number of FFT points increases from 256 to higher values, thereby enhancing the accuracy of the calculated normalized amplitudes of the frequencies higher than the cutoff frequency (39.06 Hz). The frequencies lower than the cutoff frequency cannot be predicted correctly, even by increasing of the number of FFT points. When one uses a larger number of data samples than FFT points, many new, nonphysical low-amplitude frequencies are introduced (see Fig. 2). An advantage of using the same number for the data samples and the FFT points is that these new frequencies are fewer, making it easier to determine the envelope of the maximum frequencies of the signal. Figure 3 shows this envelope superimposed on top of the FFT signal. A disadvantage of using a larger number of FFT points is the existence of other low-amplitude frequencies that are not in the physical signal and thereby increase the signal processing time to resolve these frequencies. Fortunately these nonphysical frequencies can be easily detected and ignored, with the peaks of the physical frequencies found by finding the envelope of the local maxima first. The larger the number of the number of samples and FFT points, the better predicted are the frequencies and amplitudes outside of the cutoff region. The accuracy of this approach does not depend on the accuracy of the database examined, rather on the number of samples and FFT points used.

It is clear from this example that there are two spectral regions, the cutoff region where the frequencies cannot be predicted correctly (error frequencies) and a region beyond the cutoff region where physical frequencies can be predicted correctly. The value of the cutoff frequency depends on the choice of number of data samples and the sampling rate. It is important that the cutoff frequency must be less than the physical frequencies of the fluid flow variable.

Jet in Crossflow Example

The jet in crossflow (JICF) is a fundamental problem found in many practical applications. Such problems are found in the mixing of air or fuel with mainstreams in jet engine and scramjet combustors and the cooling of turbine blades. The problem of injecting a steady jet flow injected into a steady crossflow has been extensively investigated experimentally. Recently, researchers have proposed use of unsteady or forced jets in crossflow (FJICF) to enhance the mixing process[20–22] of the jet into the mainstream flow.

In the current study, the JICF problem is solved numerically using Fluent 4.5.6 software.[23] A first-order upwind scheme with the SIMPLE algorithm is used in these calculations. The number of inner iteration for each time is 20. The Navier–Stokes equations are solved, with turbulence effects modeled using the k–ε turbulence model. A three-dimensional Cartesian computational domain, $x/d = 100$, $y/d = 18$, and $z/d = 18$, is considered, where d is the diameter of the jet. For simplicity of gridding, the jet is assumed to have a square cross section with an equivalent hydraulic diameter of 4.57 mm. The number of grid points is half a million, $200 \times 50 \times 50$ in the x, y, and z directions, respectively. The grid is clustered in the axial direction around the jet where gradients are expected to be large. A grid study was performed in an earlier work,[24] with no change in penetration or mixing observed using a finer mesh. The boundary conditions (BC) are as follows: 1) specified inlet velocities of the jet and the mainstream fluids, where the inlet crossflow velocity is 10 m/s while the jet-exit velocity is calculated from the following expression as

$$u = 30 + 30 \sin(2\pi 400t) \tag{10}$$

2) zero pressure gradient at $x = L$; 3) no-slip BCs on the lower wall ($y = 0$); and 4) symmetry BCs on upper and sidewalls ($y = H$,

$z = 0, W$), where L, H, and W are the length, height, and width of the computational flow channel, respectively. The initial condition for the axial velocity equals the mainstream inlet velocity. The initial condition of all other variables is zero.

The ratio of the momentum flux of the jet to the momentum flux of the mainstream J is 9 in the presented case. The working fluid for both the mainstream and the jet is air. Both flows are treated as ideal gases at 300 K. If no reaction is present, species ($Y1$) acts as an inert gas and is solved for from the species transport equation. In real experiments, injected jet air is seeded with smoke or particles to differentiate it from the mainstream air. In this study, the jet air species ($Y1$) is called the seed gas, and it is measured in terms of mass fraction (MF). The air of the jet will be called the seed from now on. Figure 4 shows the average distribution of the seed mass fraction in the symmetry plane ($z/d = 9$) after 1200 time steps. The jet bends in the mainstream flow direction, and the local value of the seed mass fraction decreases in the x direction.

Figure 5 shows the normalized rms residual change[23] over the domain for the u-, v-, w-momentum equations and the mass diffusion equation (MF) obtained from a Fluent simulation. These residual are plotted with the time step and not with iteration. The residuals oscillate largely because of the imposed unsteady boundary condition. The maximum values correspond to the maximum value of the jet-exit velocity (60 m/s), whereas the minimum values of the residual correspond to the minimum value of the jet-exit velocity (zero-velocity value). It is not easy therefore to evaluate from the residual, when the numerical solution has converged. The oscillation of the seed mass fraction residual is larger than that of the momenta residuals. Although there is no obvious criterion when convergence is reached, it can be suggested from visual check that 250–300 time steps are enough to reach the converged solution. To apply the suggested FFT convergence criterion, time-domain data of variables of interest need to be collected. U, v, w, and MF variable data are collected for 1000 time steps at five different locations upstream and downstream of the jet injection location, as shown in Fig. 6 and presented in Table 2. Figure 7 shows an FFT analysis of the seed mass fraction at point 4, $30d$ downstream of the jet. Figure 7a shows the seed mass fraction variable in the time domain. The seed mass fraction starts with a zero value at $t_s = 0$ and increases with time before decreasing to a uniform value at $t \approx 150$. The seed mass fraction increases as the jet trajectory reaches point 4 and then decreases as the jet core passes this location. This figure might suggest that after

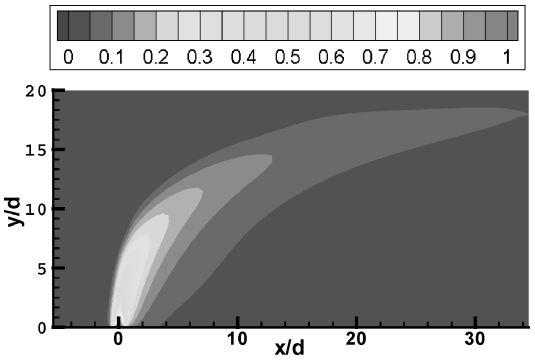

Fig. 4 Time-averaged distribution of the seed mass fraction in the forced jet in crossflow ($J = 9$ and frequency of the jet = 400 Hz).

Table 2 Point locations in JICF computational domain

Point	x/d	y/d	Note
$p1$	−8.84	5.72	Near inlet of mainstream
$p2$	0.25	5.72	Downstream
$p3$	4.81	5.72	Downstream
$p4$	30.48	5.72	Downstream
$p5$	88.29	5.72	Near exit

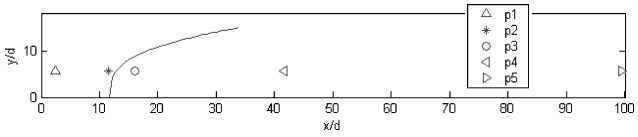

Fig. 6 Schematic of the FJICF domain showing the physical locations of the five points under investigation.

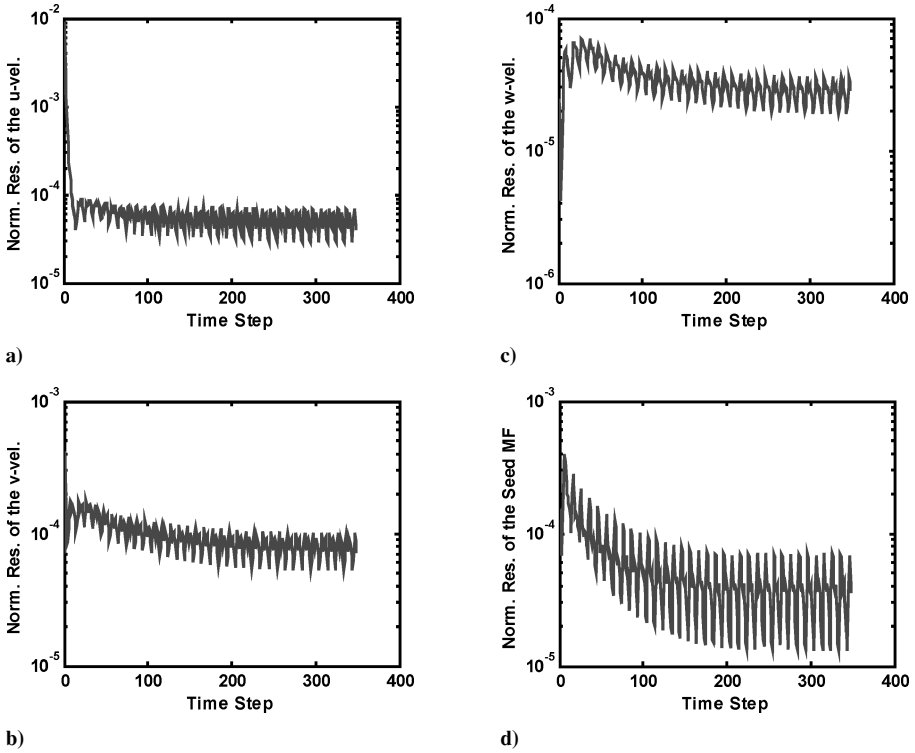

Fig. 5 Normalized residuals of the forced jet in crossflow for the a) u-momentum equation, b) v-momentum equation, c) w-momentum equation, and d) seed mass fraction equation.

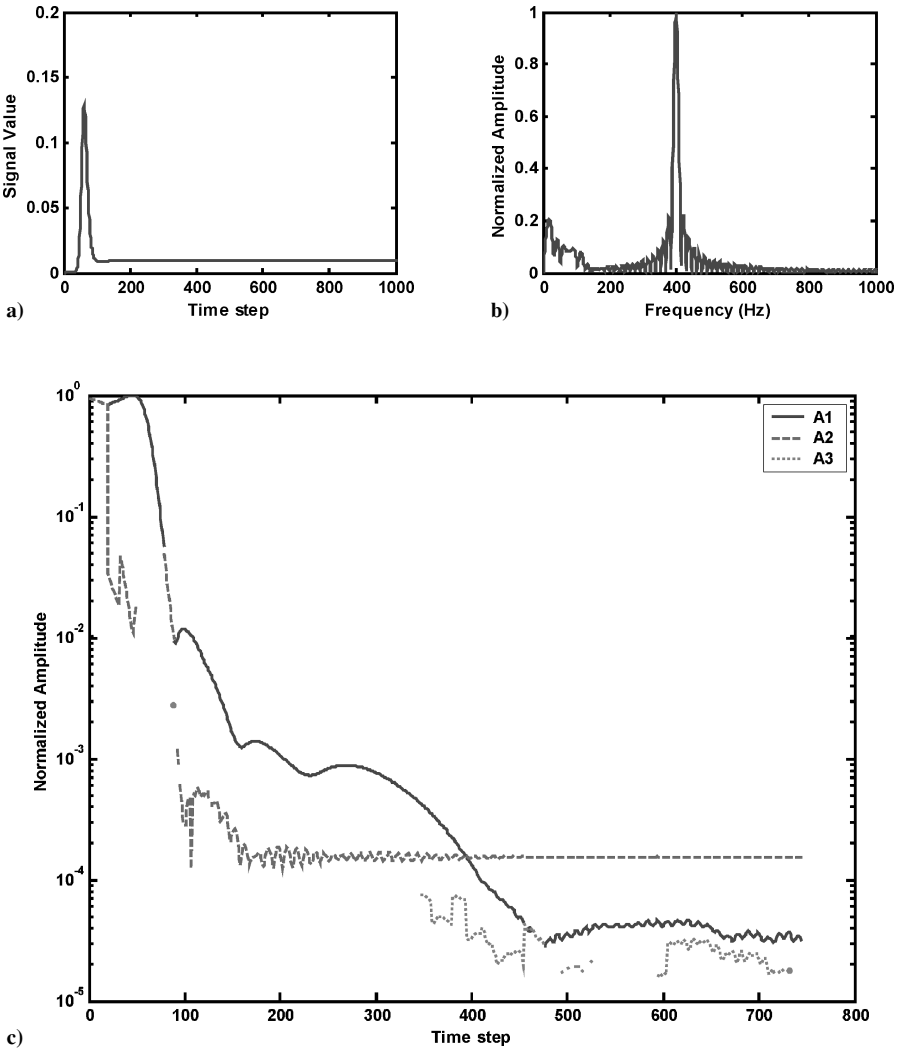

Fig. 7 FFT convergence analysis of seed MF at point 4: a) signal in the time domain; b) frequency domain; and c) history of A_1, A_2, and A_3 normalized amplitudes.

the flow transient is passed, the number of time steps needed to reach convergence is about 150 and there is no unsteady behavior beyond this time step. A similar conclusion could be drawn from Fig. 5d, where the solution at the same time step "looks periodic." The FFT convergence analysis is applied to the seed mass fraction signal at point 4. Figure 7b shows the frequency analysis of the last segment of data samples that starts with $t_s = 744$ and ends with $t = 1000$ at point 4. It is clear that a frequency of 400 Hz is found at this point, corresponding to the imposed jet forcing frequency. A closer look frequently reveals 800- and 1200 (not shown)-Hz harmonics are present but of significantly smaller amplitude.

The maximum frequency that can be captured is based on the time step used. In the current calculations, the time step is 2.5E-4 s; therefore, frequencies up to 2000 Hz can be captured. The number of data samples used in each FFT calculation is 256 points, and the number of FFT points is 2^{11}. The cutoff frequency in this case is 31.2 Hz. There are three important normalized amplitudes (A_1, A_2, and A_3) that have to be considered; A_1 corresponds to the error frequency f_1, A_2 corresponds to the primary or dominant physical frequency f_2, and A_3 corresponds to the secondary physical frequency.

To ensure that a numerical solution is converged all over the entire domain, one should ideally sample all dependent flow variables at many locations throughout the computational domain, but this is not practical. A more reasonable approach is to examine selected variables at several key locations. The choice of sampling variables and locations requires an intelligent examination of the problem under study. If a convergence check is needed all over the domain, it is better to select the locations of sampling far away from the source of disturbances as they appear to be the slowest to converge. Although the disturbance is larger near the jet, the frequency content is largely the same over the entire domain. The advantage of the FFT convergence criterion is that it can detect very small changes in the signal through an examination of its frequency and amplitude content.

The amplitude time histories for the three strongest modes (A_1, A_2, and A_3) at point 4 are shown in Fig. 7c. The frequency of the two strongest physical modes varies strongly with time early in the iteration process. The amplitude of the secondary physical frequency tends to be more stable. The first physical or dominant frequency reaches its converged value before the second largest physical frequency in most cases and at a time slightly larger than that needed by the signal to reach a uniform value ($t_s = 150$). At point 4, the amplitude of the error frequency A_1 decreases with time and drops below the amplitude of the dominant physical frequency after $t_s = 396$. It reaches a nearly uniform value after $t_s = 460$. The amplitude of the error frequency is about 20% of the dominant mode after $t_s = 500$, but additional time steps are needed to sure that the slight rise does not impact the solution and is therefore continued until t_s is about 750. At most time steps, the second largest physical frequency has a value that is less than 10% of the maximum amplitude. Therefore, because A_3 is below a threshold, one does not have to consider it any more.

The amplitude analysis in the early iteration process, $t < 100$, needs more clarification. At the very beginning, the error frequency shifts a little and is out of the cutoff region. As mentioned earlier,

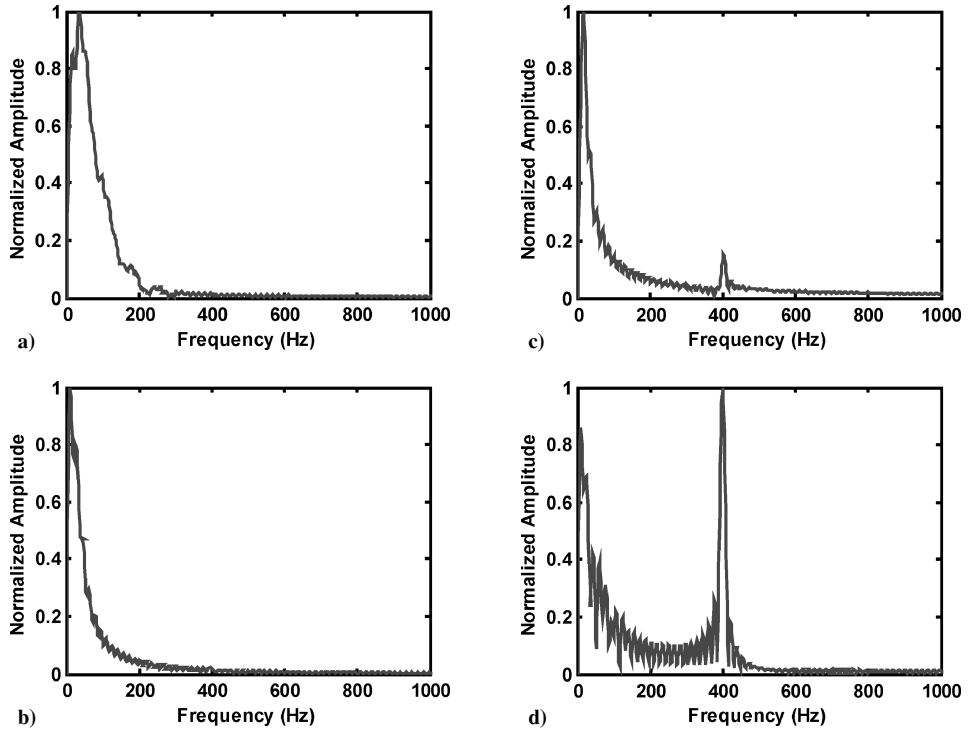

Fig. 8 FFT analysis of the seed MF at point 4 using 256 data samples starting at a) $t = 1$, b) $t = 101$, c) $t = 201$, and d) $t = 401$.

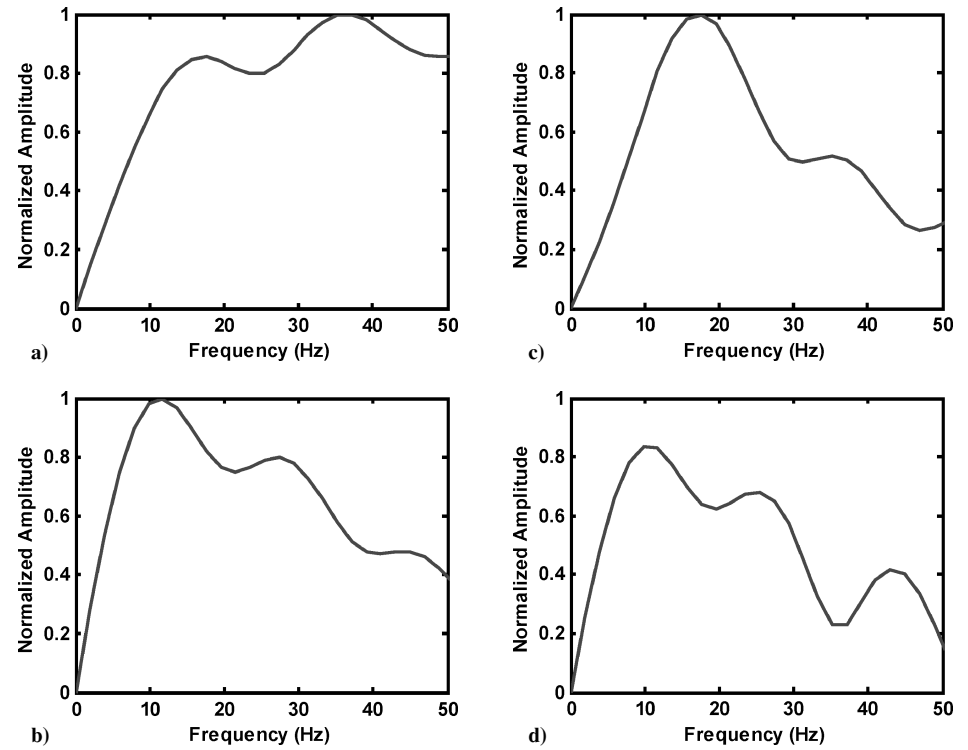

Fig. 9 Enlarged view of low-frequency region of the FFT analysis of the seed MF at point 4 using 256 data samples starting at a) $t = 1$, b) $t = 101$, c) $t = 201$, and d) $t = 401$.

this arises when the number of FFT points is higher than the number of data samples. The written code considers this amplitude as the amplitude of the dominant frequency A_2, and there is no detected frequency in the cutoff region. The amplitude of the error frequency A_1 is then assigned a value of zero. For example, as seen in Fig. 6c, after about 20 time steps the error frequency shifts out of the cutoff region, and the FFT detects this error frequency as a small amplitude signal A_2 in the physical frequency region before it disappears. After about $t_s = 80$, the error frequency is detected outside of cutoff region ($A_1 = 0$, as discussed before), but after $t_s = 90$ it returns back to the cutoff region. These observations are deduced from the continuous behavior of A_1. Figures 8 and 9, discussed next, will make these observations clearer.

To show the development of different modal amplitudes with initial sampling time t, data samples that start at four different time steps of 1, 101, 201, and 401, respectively, will be examined. The frequency analysis of each data segment is shown in Figs. 8 and 9. The number of data samples and FFT points are the same as before. For each of the first two segments of data (Figs. 8a and 8b), the error frequency is the dominant mode, and there are no significant

Table 3 Sampling summary vs point location for the JICF study

Variable	Location	Convergence iteration
MF	4	470
MF	3	320
MF	5	1000
u	4	450
v	4	550

physical frequencies. The error frequency is slightly higher than the cutoff frequency as shown in Figs. 8a and 9a. It can be concluded from Fig. 7c that the amplitude of the error frequency at $t_s = 101$ is lower than that of the first time step. After $t_s = 200$, the 400-Hz frequency appears and has an amplitude about 18% of that of the error frequency. The amplitude of the error frequency is lower than that at $t_s = 101$. At the segment that starts with $t_s = 401$, the 400-Hz mode has an amplitude that is higher than the error frequency, and the solution proceeds monotonically to convergence. From Fig. 8, attention should be made in the selection of the appropriate time step to stop calculating and start collecting data for FFT processing. Finally, a summary of the effect of point location and flowfield variable on the time to converge, as determined by the FFT-based criteria, is shown in Table 3. The time to converge is largely independent of choice of flow variable but is dependent on the distance from the primary flow disturbance. The convergence time obtained by examining different flow variables is largely obvious. In a flow dominated by a mainstream direction, the u variable will be least disturbed and converge the quickest. The greater disturbance of the primary flow variables by the natural or imposed disturbance the greater the time to converge. In any case, these times are larger than than the time (200 to 250) one would select from the data shown in Fig. 5.

Flame Holder Example

Flame holders are used to stabilize premixed flames in the afterburners of many military jet engines by introducing a surface from which a recirculation zone can be established. Frequently, flame holders can be represented as bodies of triangular cross section, with the apex pointing into the onset flow. The flow behind a triangular bluff body has been calculated using the upwinding based time-dependent Navier–Stokes solver (UTNS) code developed by Choi.[25] The unsteady Navier–Stokes equations were solved using different turbulence models. Madabushi et al.[16] used the same code to study six different cases of flow behind the triangular bluff body and found that the k–ε model with wall functions gave the best overall comparison with the measured centerline data done by Sjunnesson et al.[26] The k–ε model is used in the present study. The bluff body is an equilateral triangular cylinder with each side being 40 mm. The computational domain is about five times the length of the triangular side upstream and 20 times in the downstream direction. The height is three times the length of the triangular base. A nonuniform mesh of 17,600 grid points is used in the calculations. Finer grids were examined[25] and found to have no effect on the predicted Strouhal number. The no-slip boundary condition is applied on the walls of the triangular flame holder. Stagnation temperatures and pressures values are specified at the inlet. At the exit, the static pressure is specified while extrapolating the other variables. The inlet velocity is about 31 m/s with inlet Reynolds number of 77.5×10^3 based on the triangle base. The solution starts by solving the steady-state flow condition for 100 iterations to initialize the unsteady solution. A time step of 3.65×10^{-5} s was used for 5000 time steps. Figure 10 shows the instantaneous unsteady flowfield of the nondimensional v velocity (velocity value/speed of sound) where velocity fluctuations can be observed clearly behind the bluff body. Vortex shedding starts at one of the triangle base corners then circulates behind the base before moving downstream.

Figure 11 shows the normalized rms of the u- and v-velocity variables used to judge convergence of the flame-holder simulation. The

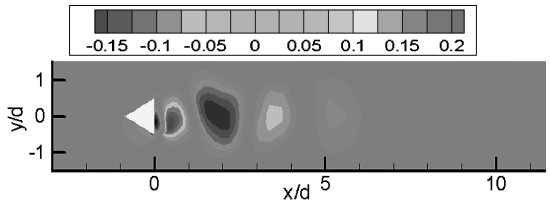

Fig. 10 Instantaneous v-velocity flow distribution over the triangular bluff body.

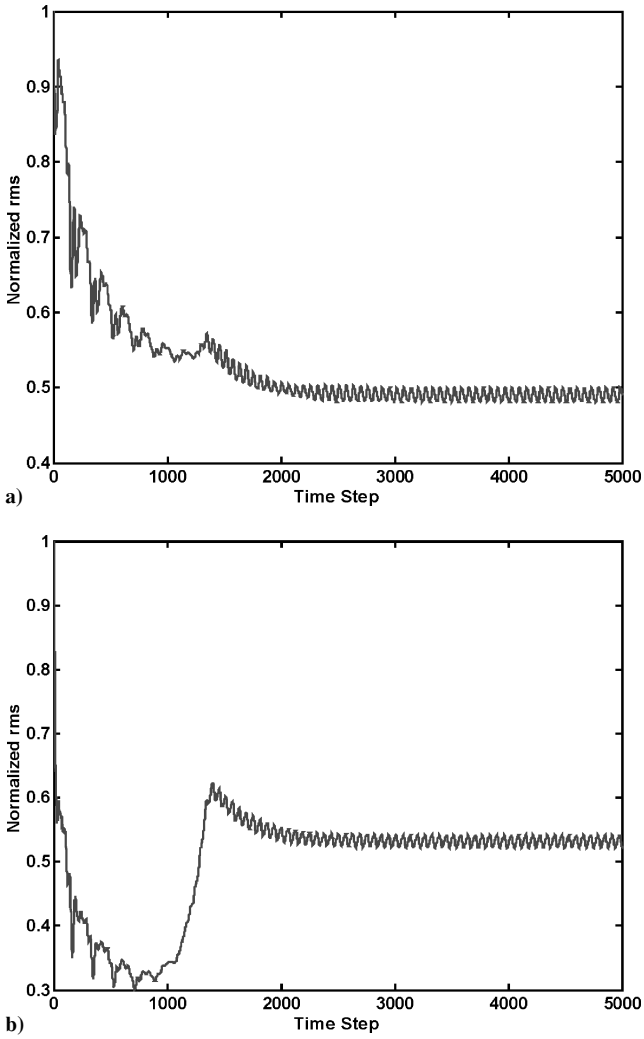

Fig. 11 Nondimensional normalized rms of the a) u velocity and b) v velocity.

residual of the v velocity has an unusual behavior as it decreases to a minimum value and then increases before reaching a periodic behavior. The sudden change is attributed to the formation and shedding of the corner vortex off of the flame holder. This is the main source of unsteadiness of this problem. Both plots suggest that convergence is reached after $t_s = 2500$. Seven points in the computational domain are chosen to investigate the applicability of the FFT convergence criterion, as shown in Fig. 11. Table 4 lists the values of the physical locations of these points. The dominant frequency, related to vortex shedding off the bluff body, is approximately 214 Hz. This corresponds to a Strouhal number of 0.276, based on the flame-holder base length and inlet velocity. For each FFT calculation, the number of the data samples is 256, and the sampling rate is four times the time steps to minimize the cutoff frequency (53.6 Hz in this case), while $N_{\text{FFT}} = 2^{11}$.

Figure 12 shows the nondimensional u-velocity time signal at point 1 upstream of the bluff body and the FFT convergence

Table 4 Point locations in flame-holder computational domain

Point	x/d	y/d	Notes
$p1$	−3.44	−0.97	Upstream
$p2$	−1.93	0.77	Upstream
$p3$	0.53	0.30	Downstream
$p4$	1.08	0.30	Downstream
$p5$	5.09	0.27	Downstream
$p6$	10.40	0.24	Downstream
$p7$	15.50	0.20	Downstream

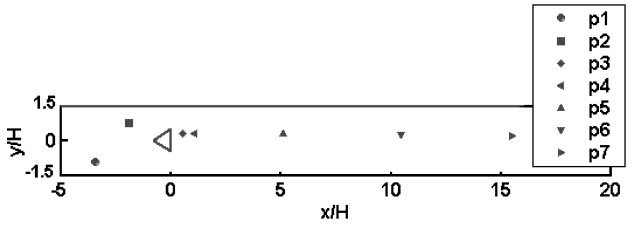

Fig. 12 Spatial location of the seven points under consideration of the flow over bluff-body problem.

analysis of this signal. Figure 13a shows the nondimensional u-velocity value in the time domain. The velocity value fluctuates largely at the beginning of the unsteady simulations, and the fluctuations decrease with time before reaching uniform value. Figure 13b shows the nondimensional u-velocity signal in the frequency domain for the last segment of data samples that starts at $t_s = 3976$. There are two strong frequencies, which are the 214 Hz mode and its first harmonic. The change of the normalized amplitudes A_1, A_2, and A_3 with time is shown in Fig. 13c. As shown, the normalized amplitude of the error frequency A_1 decreases with time until intersecting with the amplitudes of the other two frequencies. The amplitudes of the physical frequencies can increase or decrease with time depending on the initial conditions of the unsteady simulation. At point 1, A_2 and A_3 are close to each other, and after reaching convergence their fluctuations disappear. The frequencies of the two largest physical modes reach constant values before their normalized amplitudes do.

Figure 14 shows the frequency analysis of the nondimensional u velocity at point 1 for different four data segments that start at $t_s = 1$, 801, 1601, and 2401. Figure 14a shows that at the segment that starts with time step equals 1; the amplitude of the error frequency in the cutoff region has the highest amplitude. The frequencies in the out- of cutoff region are incorrect too, but they physically exist in the data samples at this time. In Fig. 14b, where the data segment (2) starts at $t_s = 801$ is shown, the error frequency in

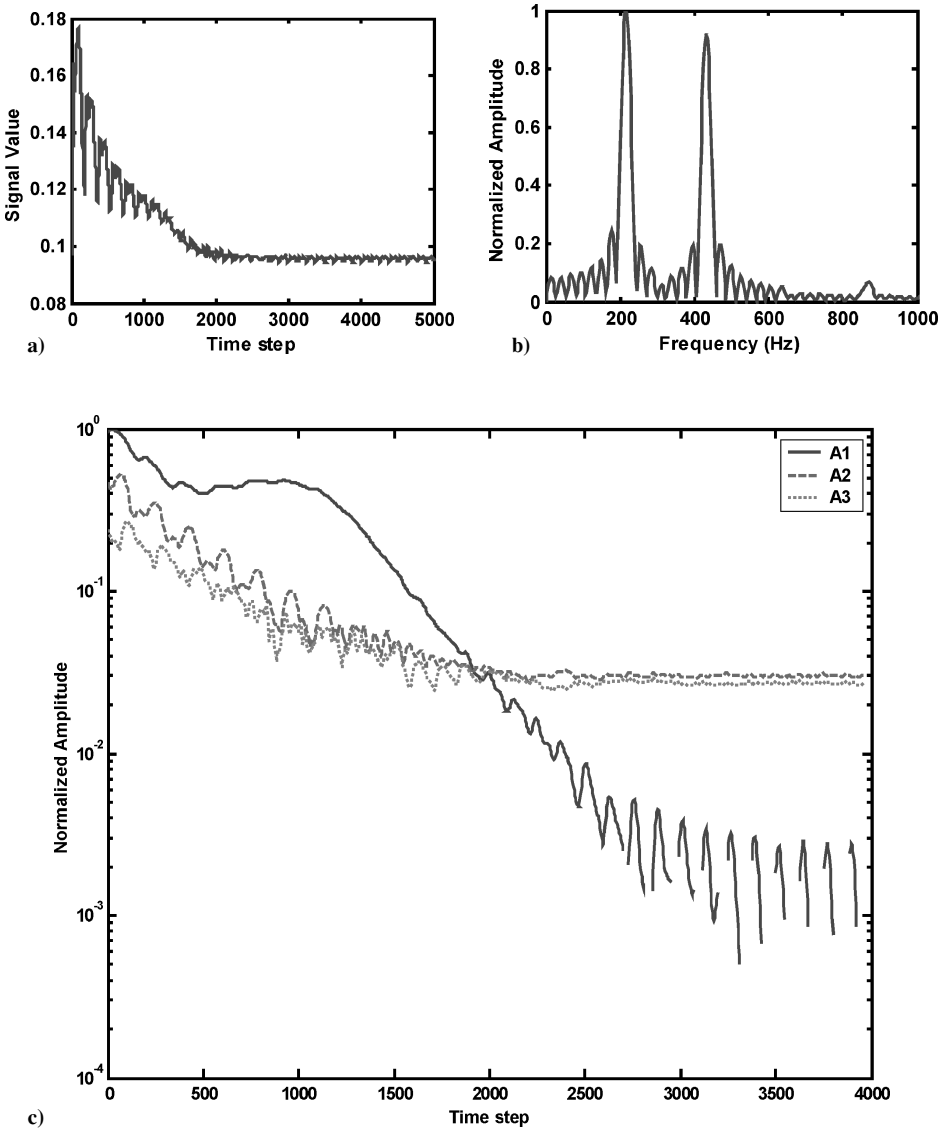

Fig. 13 FFT convergence analysis of nondimensional u-velocity at point 1: a) signal in the time domain; b) frequency domain; and c) history of A_1, A_2, and A_3 normalized amplitudes.

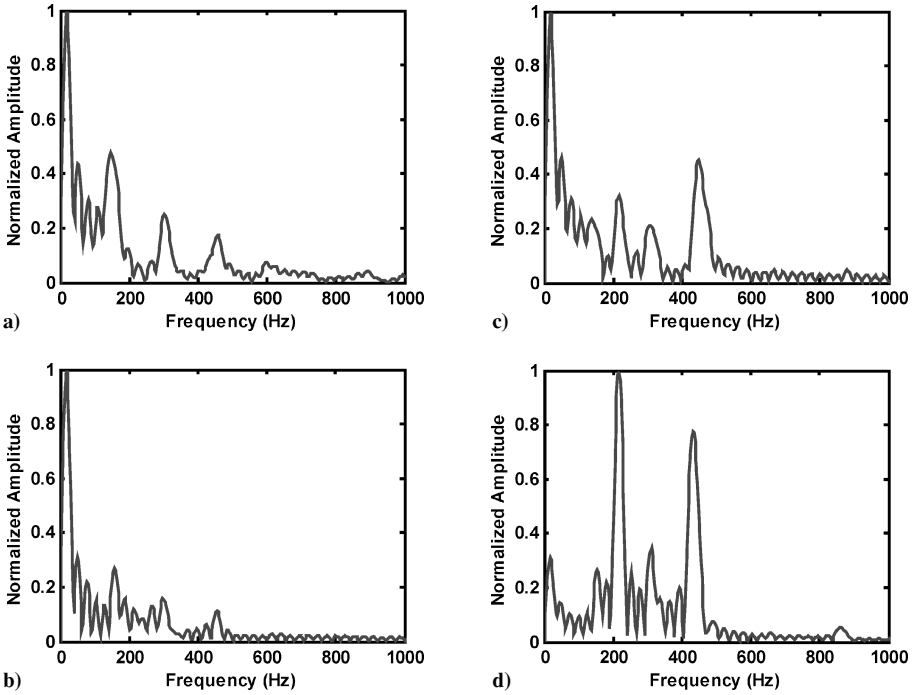

Fig. 14 FFT convergence analysis of the nondimensional u velocity at point 1 using 256 data samples at four different times. The data samples starts at a) $t_s = 1$, b) $t_s = 801$, c) $t_s = 1601$, and d) $t_s = 2401$.

Table 5 Sampling summary vs point location for the flame-holder study

Variable	Location	Convergence iteration
u	1	2700
u	4	1500
u	7	3500
v	3	1700
v	4	1700

the cutoff region still has the highest amplitude while the amplitudes of the incorrect frequencies, in the out- of cutoff region, are lower than before. For the FFT analysis of data segment (3) that starts at $t_s = 1601$, the error frequency in the cutoff region is still the highest amplitude, but the correct physical frequencies have the highest amplitudes in the out- of cutoff region and finally in the last data segment (4) that starts at $t_s = 2401$, Fig. 14d, the physical frequencies have higher amplitudes than the error frequency. The amplitude of the error frequency is the highest in the first segment and decreases until vanishing at the last segment. Again, a summary of the effect of point location and flow-field variable on the time to converge, as determined by the FFT-based criteria, is shown in Table 5. The time to converge is again largely independent of choice of flow variable but is dependent on the distance from the primary flow disturbance. In any case, these times are larger than than the time (2000) one would select from the data shown in Fig. 11.

Conclusions

An alternative convergence criterion based on the FFT analysis has been investigated. A test case has been given where a known signal is transferred from the time domain to the frequency domain to study the effect of the number of data samples, the number of points in the FFT, and the errors that associate in obtaining the frequencies and their normalized amplitudes. Two different problems, which are the forced jet in crossflow and flow over a triangular flame holder, have been solved using two different numerical codes to show the applicability of the FFT convergence criterion. The FFT convergence criterion is easily applied to unsteady problems. In most numerical simulations, the number of time steps required to reach a converged solution based on the FFT convergence analysis will be higher than that predicted by conventional convergence criteria. Examining only the so-called error frequency in the region lower than the cutoff frequency and the dominant physical frequency beyond the cutoff region is enough to judge convergence in problems that have a finite number of tones. The amplitude of the first dominant physical frequency is constant after reaching convergence, and the same behavior is observed for the amplitude of the secondary dominant physical frequency if its normalized value is higher than 30%. To reduce the number of computations, the FFT convergence criterion can be applied discontinuously after skipping some time steps. It is therefore suggested that one judge convergence by applying both steady and unsteady criteria, but when the unsteadiness (imposed or natural) is large enough, then the steady criteria cannot be satisfied, and the unsteady ones are used.

Acknowledgments

The authors thank Dochul Choi and Louis M. Chiappetta of the United Technologies Research Center for providing the UTNS code and their technical assistance in this work.

References

[1]Rowley, C. W., Colonius, T., and Murray, R. M., "POD Based Models of Self-Sustained Oscillations in the Flow past an Open Cavity," AIAA Paper 2000-1969, June 2000.

[2]Ukeiley, L. S., Steiner, J. M., Arunajatesan, S., Sinha, N., and Dash, S., "Low-Dimensional Description of Resonating Cavity Flow," AIAA Paper 2000-2459, June 2000.

[3]Ishikawa, H., Kiya, M., and Mochizuki, O., "POD and Wavelet Analysis of Coherent Structures in a Turbulent Mixing Layer," Japan Society of Mechanical Engineers, Paper ICFE-97-106, July 1997.

[4]Ducruix, S., and Candel, S., "External Flow Modulation in Computational Fluid Dynamics," *AIAA Journal*, Vol. 42, No. 8, 2004, pp. 1550–1558.

[5]Tang, D., Kholodar, D., Juang, J., and Dowell, E. H., "System Identification and Proper Orthogonal Decomposition Method Applied to Unsteady Aerodynamics," *AIAA Journal*, Vol. 39, No. 8, 2001, pp. 1569–1576.

[6]Roache, P. J., *Computational Fluid Dynamics*, Hermosa, Albuquerque, NM, 1976, pp. 174–179.

[7]Richtmeyer, R. D., and Morton, K. W., *Differential Methods for Initial Value Problems*, Wiley, New York, 1957, pp. 37, 44, 45, 171–176.

[8]Mitchell, Q. R., *Computational Methods in Partial Differential Equations*, Wiley, New York, 1969.

[9]Abbott, M. B., and Basco, D. R., *Computational Fluid Dynamics, An Introduction for Engineers*, Wiley, New York, 1989, pp. 67–69.

[10]Briley, W. R., "A Numerical Study of Laminar Separation Bubbles Using Navier–Stokes Equations," United Aircraft Research Lab., Rept. J110614-1, East Hartford, CT, 1971.

[11]Sangiovanni, J. J., Barber, T. J., and Syed, S. A., "Role of Hydrogen/Air Chemistry in Nozzle Performance for a Hypersonic Propulsion System," *Journal of Propulsion and Power*, Vol. 9, No. 1, 1993, pp. 134–138.

[12]Reynolds, W. C., and Hussain, A. K. M. F., "The Mechanics of an Organized Wave in Turbulent Shear Flow, Part 3: Theoretical Models and Comparison with Experiments," *Journal of Fluid Mechanics*, Vol. 54, Part 2, 1972, pp. 263–288.

[13]Speziale, C. G., "On the Decomposition of Turbulent Flow Fields for the Analysis of Coherent Structures," *Acta Mechanica*, Vol. 70, Dec. 1987, pp. 243–250.

[14]Poje, A. C., and Lumley, J. L., "A Model for Large-Scale Structures in Turbulent Shear Flows," *Journal of Fluid Mechanics*, Vol. 285, 1995, pp. 349–369.

[15]Raffoul, C. N., Nejad, A. S., Gould, R. D., and Spring, S. A., "An Experimental and Numerical Study of the Isothermal Flowfield Behind a Bluff Body Flameholder," *Transactions of the ASME*, Vol. 119, April 1997, pp. 328–339.

[16]Madabhushi, R. K., Choi, D., and Barber, T. J., "Unsteady Simulations of Turbulent Flow Behind a Triangular Bluff Body," AIAA Paper 97-3182, July 1997.

[17]Proakis, J. G., and Manolakis, D. G., *Introduction to Digital Signal Processing*, Macmillan, New York, 1988, Chap. 9.

[18]Lathi, B. P., *Signal Processing and Linear Systems*, Cambridge Press, Berkeley, CA, 1998, Chap. 8.

[19]Ludeman, C. L., *Fundamentals of Digital Signal Processing*, Harper and Row, New York, 1986, Chap. 6.

[20]Johari, H., Pacheco-Tougas, M., and Hermanson, J. C., "Penetration and Mixing of Fully Modulated Turbulent Jets in Crossflow," *AIAA Journal*, Vol. 37, No. 7, 1999, pp. 842–850.

[21]M'Closkey, R. T., King, J. M., Cortelezzi, L., and Karagozian, A. R., "The Actively Controlled Jet in Crossflow," *Journal of Fluid Mechanics*, Vol. 452, 2002, pp. 325–335.

[22]Shapiro, S., King, J. M., and Karagozian, A. R., and M'Closkey, R. T., "Optimization of Controlled Jets in Crossflow," AIAA Paper 2003-0634, Jan. 2003.

[23]Fluent 4.5 Documentation, Fluent, Inc., Lebanon, NH, Nov. 2000.

[24]Barber, T. J., and Ahmed, M., "Mixing and Frequency Analyses of a Forced Jet in Crossflow," AIAA Paper 2004-0095, Jan. 2004.

[25]Choi, D., "A Navier–Stokes Analysis of Film Cooling in a Turbine Blade," AIAA Paper 93-0158, Jan. 1993.

[26]Sjunnesson, A., Nelson, C., and Max, E., "LDA Measurement of Velocity and Turbulence in a Bluff Body Stabilized Flame," American Society of Mechanical Engineers, 4th International Conf. on Laser Anemometry Advances and Applications, Aug. 1991.

P. Givi
Associate Editor